Article:
Mottram, L.M., Dixon Wilkins, M.C., Blackburn, L.R. et al. (2020) A feasibility investigation of laboratory based X-ray absorption spectroscopy in support of nuclear waste management. MRS Advances, 5 (1-2). pp. 27-35.

https://doi.org/10.1557/adv.2020.44

MRS Advances

A Feasibility Investigation of Laboratory Based X-ray Absorption Spectroscopy in Support of Nuclear Waste Management

L.M. Mottram, M.C. Dixon Wilkins, L.R. Blackburn, T. Oulton, M.C. Stennett, S.K. Sun, C.L. Corkhill, and N.C. Hyatt

Immobilisation Science Laboratory, University of Sheffield, Department of Materials Science and Engineering, Sir Robert Hadfield Building, Mappin Street, S13JD, UK

ABSTRACT

X-ray Absorption Spectroscopy is a technique of fundamental importance in nuclear waste management, as an element specific probe of speciation, which governs radionuclide solubility, immobilisation and migration. Here, we exploit recent developments in laboratory instrumentation for X-ray Absorption Spectroscopy, based on a Rowland circle geometry with a spherically bent crystal analyser, to demonstrate speciation in prototype ceramic and glass-ceramic waste forms. Laboratory and synchrotron XANES data acquired from the same materials, at the Ce and U L_3 edges, were found to be in excellent quantitative agreement. We establish that analysable laboratory XANES data may be acquired, and interpreted for speciation, even from quite dilute absorber concentrations of a few mol%, albeit with data acquisition times of several hours. For materials with suitable absorber concentrations, this approach will enable routine element specific speciation studies to support rapid optimisation of radioactive waste forms and analysis of radiological materials in a purpose designed laboratory, without the risk associated with transport and manipulation at a synchrotron radiation facility.

INTRODUCTION

As an element specific probe of speciation X-ray absorption spectroscopy (XAS) finds ubiquitous and powerful application in the field of nuclear waste management, in particular in the development of waste form materials[1-16]. The fundamental requirement for a tunable broadband source of high brilliance X-rays, has, hitherto, generally required exploitation of synchrotron radiation sources for application of XAS techniques. However, recent advances in laboratory XAS instrumentation, exploiting spherically bent crystal analysers (SBCAs) in Rowland circle geometry, or bent cylindrical analysers in von Hamos geometry[17-26]. The use of SBCAs generally

delivers higher spectral resolution in the region of the X-ray Absorption Near Edge Structure (XANES), but the requirement to work close to back scattering geometry requires several monochromator crystals to cover the range 5 – 18 keV, and a precision motor driven system to maintain optical alignment[17-21]. In contrast, the von Hamos geometry utilises only a single bent crystal analyser and does not necessarily require movement of components for acquisition of spectra, however, the achievable resolution in the XANES region is comparatively lower[22-26]. These developments in instrumentation offer the potential to transform the application of XAS techniques in many scientific fields, by enabling routine studies of materials in which the absorbing element is moderately dilute to concentrated. With regard to research involving radioactive materials, laboratory instrumentation offers the inherent advantage of allowing characterisation to be completed, or at least preliminary investigation performed, without the need to move samples to the synchrotron source, reducing the risk, cost and timescale of research. Recently, Jahrman *et al.*, reported the first Ce and U L_3 XANES from reference compounds, achieved with a laboratory spectrometer using a SBCA[20]. Bes *et al* developed this approach with the report of laboratory U L_3 XANES data acquired from UO_2, UO_3 and KUO_3[27]. In this contribution we present the results of our preliminary investigation in the application of laboratory XAS to the characterisation of element speciation in materials for radioactive waste immobilisation.

EXPERIMENTAL

The spectrometer utilised in this study was an EasyXAFS 100 extended spectrometer, produced by EasyXAFS LLC, Seattle, USA, based on the design of Seidler et al [17-20]. The instrument is the first of its kind to be installed and commissioned in the UK, within the HADES facility at the University of Sheffield. The optical arrangement of the spectrometer is shown in Figure 1 and is based on a Rowland circle of 1m diameter. Energy scanning involves symmetrical movement of source and detector on a linear translation stage to increment Bragg angle steps. The X-ray source is a low power, air cooled, X-ray tube with a maximum output of 100 W. The sample is located in front of a Hitatchi Vortex Silicon Drift Detector (SDD), with a 5 mm exit slit to minimise stray scatter. The energy resolution of the SDD is ca. 140 eV, enabling rejection of the harmonic content of the incident beam and background scatter. Alignment of source, SBCA and detector is maintained by steering bars. With robust initial SBCA alignment, change over and alignment of SBCAs is straightforward and can be achieved in 30 minutes or less, the spectrometer is also easily adapted to perform X-ray Emission Spectroscopy experiments.

Laboratory Ce and U L_3 edge XANES data were acquired in transmission mode using, respectively the (422) and (1266) harmonic of a Si (211) SBCA. A step size of 0.75 eV and count time of 10s / step were used in the XANES region. A He flight path (welded steel enclosure with kapton windows) was employed to minimise air scatter and absorption. Data were acquired with ($I_t(E)$) and without the sample ($I_0(E)$), using the same scan parameters. The absolute energy scale was calibrated using a Cr foil (E_0 = 5989.00 eV)[29] or Y_2O_3 (E_0 = 17042.30 eV) reference, for the Ce L_3 and U L_3 edges respectively (E_0 set as first peak in first derivative). The Bragg angle, θ_m, corresponding to the first peak in the derivative spectrum of the reference, was set equivalent $E_c = E_0$, enabling the energy scale to be calibrated according to:

$$E_c = \frac{E_m sin(\theta)}{sin(\theta + \Delta\theta)}$$

where, E_m is the measured energy, E_c the calibrated energy, and $\Delta\theta$ is the difference between the measured Bragg angle at E_c and at E_m

Synchrotron Ce and U L_3 edge XANES data were acquired in transmission mode at beamline B18, Diamond Light Source, configured with a collimating mirror, a fixed-exit double crystal Si(111) monochromator, and a double toroidal focussing mirror. The step size in the XANES region was 0.5 eV for all measurements. The absolute energy scale was calibrated using a Cr foil (E_0 = 5989.00 eV) or Y foil (E_0 = 17038.00 eV)[29] reference, for the Ce L_3 and U L_3 edges respectively. Additionally, we calibrated the E_0 of our Y_2O_3 secondary standard against an Y foil utilising the BMM beamline, NSLS II; data were acquired in transmission mode, using a Si (111) monochromator, utilising a harmonic rejection mirror and toroidal focusing mirror. Incident and transmitted beam intensities were measured using ionization chambers, filled with mixtures of He and Ar or N_2, operated in a stable region of their I/V curve, for synchrotron data.

Samples were prepared for XANES analysis by diluting the material to be investigated in polyethylene glycol to yield a thickness of $\mu x = 1$. All XANES data were dead time corrected and processed in Athena using standard background subtraction and normalisation procedures[30].

The materials investigated by Ce and U L_3 XANES were CeO_2, $CePO_4$, $Ca_{0.75}ZrCe_{0.25}Ti_{1.5}Al_{0.5}O_7$, UTi_2O_6, $U_{0.55}Yb_{0.45}Ti_2O_6$, UO_3 and a brannerite glass ceramic comprising nominally UTi_2O_6 (50 wt%) crystallised in $Na_2AlBSi_2O_6$ glass (50 wt%). CeO_2, $CePO_4$, UTi_2O_6, and $U_{0.55}Yb_{0.45}Ti_2O_6$ were synthesized as reported previously[2,10,31]. UO_3 was utilized as stock material, originally produced by British Drug Houses. $Ca_{0.75}Ce_{0.25}ZrTi_{1.5}Al_{0.5}O_7$ was synthesized from stoichiometric quantities of $CaTiO_3$, TiO_2, CeO_2 and Al_2O_3, ball milled for 30 min at 300 r.p.m.; the mixture was pressed as a 13 mm pellet and subject to reaction – sintering at 1350°C for 4h in air. All materials were confirmed to be single phase by powder X-ray diffraction. The brannerite glass-ceramic was synthesized by first calcining a homogenized and stoichiometric mixture of SiO_2, H_3BO_3, Na_2CO_3, and Al_2O_3 at 600 °C for 6 hours, this was then ball milled with the required quantity of UO_2 and TiO_2 at 300 r.p.m. for 30 min. The recovered powder batch was pressed into 13 mm pellets and heat treated at 1200°C for 12h under Ar gas flow. X-ray diffraction analysis showed the material to comprise UTi_2O_6 and an amorphous phase (evident from diffuse scattering), plus trace UO_2. SEM/EDX analysis demonstrated U to be partitioned primarily into the brannerite ceramic phase, but with minor uptake into the glass phase – estimated as 2.5 wt% UO_2 by EDX analysis.

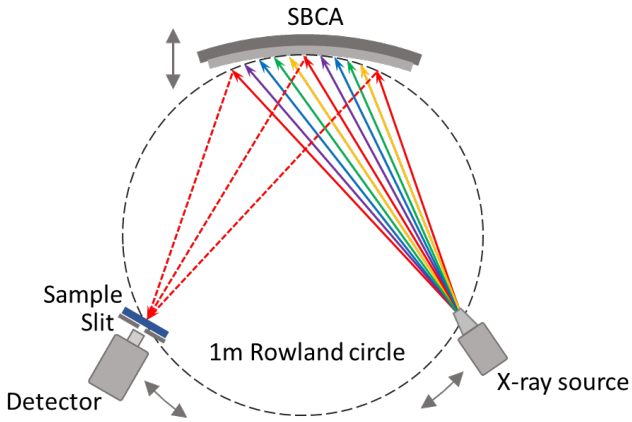

Fig. 1: Schematic representation of Rowland circle geometry for laboratory transmission X-ray Absorption Spectroscopy, as described in the text; note, the He flight path (a welded steel enclosure with kapton windows) is not shown.

RESULTS AND DISCUSSION

Ce L_3 XANES

Ce is often used as a Pu surrogate in development of ceramic, glass, and glass-ceramic waste forms, given that both elements adopt oxidation states $Ce^{3/4+}$ and $Pu^{3/4+}$, which controls partitioning in the phase assemblage[2,6-8,10]. Consequently, routine determination of $Ce^{3+}/^{4+}$ ratios in prototype waste form materials is essential for understanding surrogate partitioning mechanisms, governed by redox behavior and hence the processing conditions of the material. Figure 1 shows a comparison of laboratory and synchrotron XANES data acquired at the Ce L_3 edge of $CePO_4$ and CeO_2 reference compounds. The laboratory data sets were each acquired in 3h, whereas the synchrotron data sets were each acquired in 10 minutes. The laboratory and synchrotron data of the reference compounds are in excellent overall agreement, although some minor variation in the intensity of XANES features can be discerned. These variations are caused by small differences in the thickness of the different individual samples prepared for the laboratory and synchrotron experiments, combined with some contribution from "leakage" effects as described below. The Ce L_3 absorption edge of Ce^{3+} species, such as in $CePO_4$, is characterized by a single intense feature attributed to the transition from an initial $2p^64f^15d^0$ state to a $2p^54f^15d^1$ final state [8,10,30-32]. In contrast the absorption edge of Ce^{4+} species, such as in CeO_2, is characterized by three features attributed to the transition from an initial $2p^64f^05d^0$ state to a $2p^54f^25d^1\underline{L}^2$, $2p^54f^15d^1\underline{L}^1$, and $2p^54f^05d^1$ final states, in order of increasing energy[8,10,31-33]. These features are well resolved in the laboratory XANES data and led us to investigate the potential for speciation of an unknown. Figure 1 also shows Ce L_3 edge XANES data acquired from a zirconolite ceramic with composition $Ca_{0.75}Ce_{0.25}ZrTi_{1.5}Al_{0.5}O_7$ developed for immobilization of UK separated civil plutonium. These data are the summation of 10 individual data sets, with a total data collection time of ca. 8h; note that the concentration of the Ce absorber species is only 2.3 mol%.

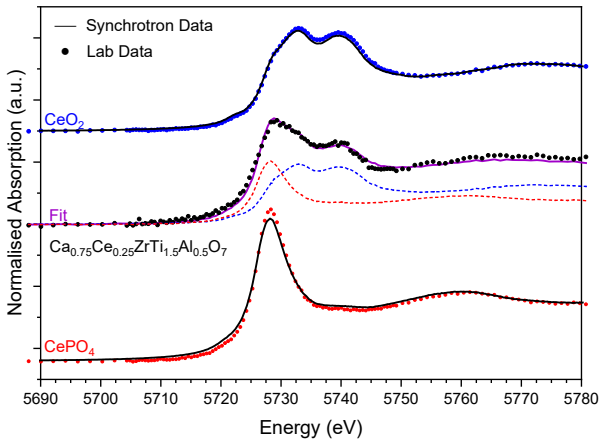

Fig. 2: Laboratory Ce L_3 XANES of $CePO_4$ (Ce^{3+}) and CeO_2 (Ce^{4+}) reference compounds (solid points) and linear combination fit (solid pink line)) to Ce L_3 XANES data of $Ca_{0.75}Ce_{0.25}ZrTi_{1.5}Al_{0.5}O_7$ (solid points), contributions of reference compounds to linear combination fit are shown by dotted lines, see text for details; synchrotron data are shown as a solid black line.

X-ray powder diffraction and SEM / EDX analysis of ceramic $Ca_{0.75}Ce_{0.25}ZrTi_{1.5}Al_{0.5}O_7$ demonstrated the phase assemblage of this material to be 84.9 wt% zirconolite, with 13.5 wt% (Ca,Ce)TiO_3 perovskite and 1.6 wt% Al_2O_3. The Ce L_3 XANES data acquired from the zirconolite ceramic show features characteristic of both Ce^{3+} and Ce^{4+} species, by comparison with the reference compounds. Linear combination fitting of the reference spectra to that of the zirconolite ceramic afforded an estimate of 57.2 % Ce^{3+} and 42.8 % Ce^{4+} species, with the constraint of $(1 - x)$ Ce^{4+} + x Ce^{3+} = 1 (where x is the weight fraction). The fitted linear combination of $CePO_4$ and CeO_2 spectra is excellent (R factor = 0.003) and demonstrates that effective Ce speciation may be achieved using laboratory XANES with reasonable data collection time, even for quite low absorber concentrations. The presence of Ce^{3+} is consistent with the formation of a significant minor fraction of perovskite phase, in which this species is known to preferentially partition, given the identical ionic radii for Ce^{3+} and Ca^{2+} (1.48Å), with respect to the 12- co-ordinate site in the perovskite structure[34].

U L_3 XANES

Uranium shows a rich redox chemistry in the nuclear fuel cycle, involving oxidation states U^{4+}, U^{5+} and U^{6+}, which is often of critical importance in understanding structure – property – function relations in chemical and materials systems[9,13]. The investigation of uranium bearing materials at a synchrotron source is, understandably, governed by strict safety protocols relating to sample transport and experimental procedure. Routine analysis of U L_3 XANES would therefore be of considerable impact in nuclear fuel cycle research, including radioactive waste management and disposal. Figure 4 compares U L_3 laboratory and synchrotron XANES data acquired from UTi_2O_6; the data collection parameters are summarized in Table 1. Comparison of the laboratory and synchrotron XANES data shows that the near edge features are well reproduced in the laboratory data, albeit with lower signal to noise as a result of the low photon flux. However, there is some mismatch in the measured absorption in the region of the white line. Such distortions are symptomatic of sample thickness and/or "leakage" effects. In the present case, the sample was prepared to yield an effective thickness of $\mu x = 1$, with due regard to homogeneity, and thus cannot be considered to be overly thick. "Leakage" effects incorporate a multitude of signal distortions arising from the contribution to the measured transmission of harmonics, stray scatter, and the low energy tail of the monochromator function (I_{lk})[35]. Consequently, $\mu = \ln (I_0 - I_{0,lk}) / (I_t - I_{t,lk})$, and thus μ no longer strictly depends on I_0 and I_t. In simple terms, I_{lk} makes a significant contribution to the measured I_t, which is small because μ is a maximum at the white line and the sample is strongly attenuating. The data can be effectively corrected for this "leakage" effect, by measurement of $I_{0,lk}$ and $I_{t,lk}$, which is achieved by using a large detector offset, in this case 4.0°, as shown by comparison of Figure 3 and 4.

Figure 4 shows a comparison of laboratory and synchrotron U L_3 XANES acquired on reference compounds UTi_2O_6, $U_{0.55}Yb_{0.45}TiO_6$, and UO_3, with correction of laboratory data for "leakage" effects. In Figure 4, the laboratory and synchrotron data are shown as points and solid lines, respectively, and are clearly in excellent agreement. A small deviation in laboratory and synchrotron XANES data of UO_3 is apparent in the region of the white line, which is thought to arise from the fact that this sample was strongly self-attenuating. Table 1 summarises the energy E_0 associated with the X-ray

absorption edge, from laboratory and synchrotron XANES data, determined as the first peak in the first derivative. The agreement between laboratory and synchrotron determined E_0 values is remarkable, within 0.1 eV for each compound. The chemical shift range of E_0 for the reference compounds is certainly resolvable using laboratory XAS, which should enable the routine speciation of "unknown" uranium oxidation states,

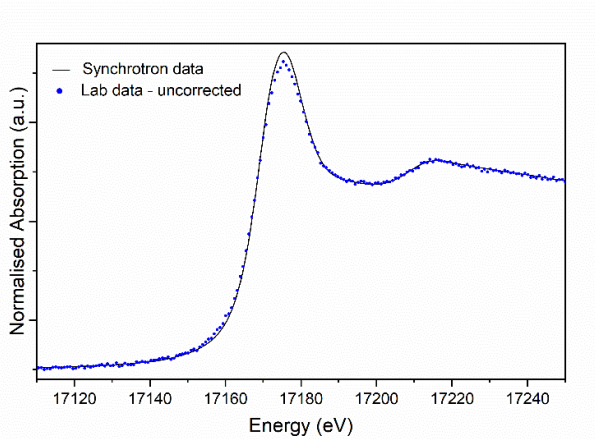

if the absorber is sufficiently concentrated. To test that hypothesis, we acquired laboratory U L_3 XANES data from a brannerite glass ceramic, comprising nominally 50wt% UTi_2O_6 crystallised in 50wt% $Na_2AlBSi_2O_6$ glass. The data and E_0, presented in Figure 4 and Table 1, are in excellent agreement with those acquired from crystalline UTi_2O_6.

Fig. 3. Comparison of laboratory and synchrotron U L_3 XANES data from UTi_2O_6, without correction of laboratory data for "leakage" effects – see text for details.

Assuming E_0 to have a linear dependence on oxidation state for the brannerite structure, then by interpolation between UTi_2O_6 and $U_{0.55}Yb_{0.45}TiO_6$, we estimate the bulk U oxidation state in the glass ceramic to be 4.2 ± 0.1. The marginally higher oxidation state compared to the bulk ceramic is thought to arise from the minor contribution of U incorporated in the glass phase as U^{5+} or U^{6+}. Note that these data also demonstrate the potential for performing U L_3 XANES speciation studies on relatively dilute absorber concentrations, using a commercially available laboratory XAS spectrometer.

Compound	U Mol%	Oxidation State	Laboratory			Synchrotron		
			No. scans	Time (h)	E_0 (eV)	No. scans	Time (min)	E_0 (eV)
UTi_2O_6	11.1	4.0+	20	15	17,164.51	3	15	17,164.65
$U_{0.55}Yb_{0.25}Ti_2O_6$	6.1	5.0+	20	15	17,166.04	3	15	17,166.15
UO_3	25.9	6.0+	20	15	17,169.47	3	15	17,169.87
UTi_2O_6 GC	2.8	4.2 (±0.1)+	20	15	17,164.65			

Table 1. Data collection parameters for laboratory and synchrotron U L_3 XANES data; precision in E_0 estimated to be ± 0.4 and ± 0.3 eV respectively; note GC – glass ceramic.

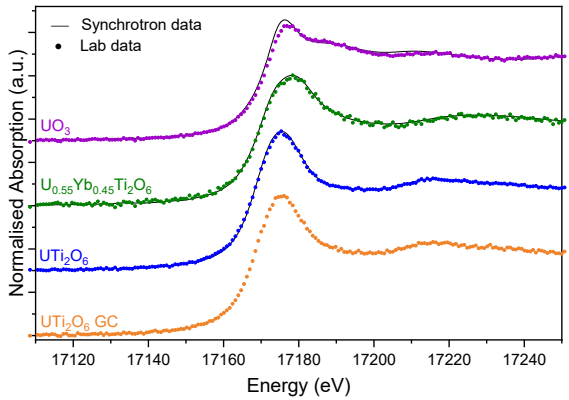

Fig 4. Comparison of laboratory (points) and synchrotron (black solid line) U L_3 XANES data from reference compounds incorporating U^{4+} – UTi_2O_6, U^{5+} – $U_{0.55}Yb_{0.45}Ti_2O_6$, U^{6+} – UO_3, and a brannerite glass ceramic with unknown U oxidation state; note: laboratory data were corrected for "leakage" effects; GC – glass ceramic.

CONCLUSIONS

Laboratory XANES at the Ce L_3 and U L_3 edge were successfully demonstrated for speciation studies in ceramic and glass-ceramic waste forms, by comparison to reference compounds. At the U L_3 edge, XANES data are susceptible to "leakage" effects which suppress the white line and XANES features, however, it is possible to correct data for this effect by measurement and subtraction of the total background scatter and harmonic contribution. The XANES features of Ce^{3+} and Ce^{4+} allow straightforward determination of these oxidation states and, by linear combination fitting of reference compounds, determination of the average of mixed oxidation states. With respect to the U L_3 edge, the chemical shift of E_0 with oxidation state, for three reference compounds, was found to be in excellent agreement between laboratory and synchrotron data. By comparison with the chemical shift of these reference compounds bulk speciation of U was effectively achieved for a brannerite glass-ceramic. This investigation also demonstrated the application of laboratory XANES to materials with absorber concentrations of only a few mol%, which is relevant to optimization of the materials chemistry of waste form materials through routine characterisation, albeit with data acquisition times of several hours. In this context, laboratory XANES is of particular utility in enabling the analysis of radiological materials within a dedicated hot lab, without necessitating transport to a synchrotron radiation facility, for which there is a significant administrative overhead, and very stringent safety controls, even for kBq quantities of uranium and thorium.

ACKNOWLEDGEMENTS

We are grateful for financial support from the Nuclear Decommissioning Authority and EPSRC under grant numbers EP/M026566/1, EP/S01019X/1, EP/N017870/1 and EP/R511754/1. This research utilised the HADES / MIDAS facility at The University of Sheffield established with financial support from EPSRC and BEIS, under grant

EP/T011424/1. We gratefully acknowledge G.T. Seidler and D.R. Mortensen for useful discussions in support of this study. This research was performed, in part, at Diamond Light Source, Beamline B18, with beamtime awarded under proposal SP17243. This research used resources [or insert beamline if applicable] of the National Synchrotron Light Source II, a U.S. Department of Energy (DOE) Office of Science User Facility operated for the DOE Office of Science by Brookhaven National Laboratory under Contract No. DE-SC0012704.

References

1. D.J. Bailey, M.C. Stennett, A.R. Mason, N.C. Hyatt, J. Nucl. Mater., **503**, 164 (2018).
2. D.J. Bailey, M.C. Stennett, B. Ravel, D. Grolimund, N.C. Hyatt, RSC Advances, **8**, 2092 (2018).
3. D.S. Patil, M. Konale, M. Gabel, O.K. Neill, J.V. Crum, A. Goel, M.C. Stennett, N.C. Hyatt, J.S. McCloy, J. Nucl. Mater., **510**, 539 (2018).
4. K. Joseph, M.C. Stennett, N.C. Hyatt, R. Asuvathraman, C.L. Dube, A.S. Gandy, K.V.G. Kutty, K. Jolley, P.R.V. Rao, R. Smith, J. Nucl. Mater., **494**, 342 (2017).
5. M.A. Kim, J.H. Song, W. Um, N. Hyatt, S.K. Sun, J. Heo, Ceram. Int., **43**, 4687 (2017).
6. C.L. Corkhill, D.J. Bailey, F.Y, Tocino, M.C. Stennett, J.A. Miller, J.L. Provis, K.P. Travis, N.C. Hyatt, ACS Appl. Mater. Interf., **8**, 20562 (2016).
7. J. Squire, E.R. Maddrell, N.C. Hyatt, M.C. Stennett, Int. J. Appl. Tech., **12**, 92 (2015).
8. N.C. Hyatt, R.R. Schwarz, P.A. Bingham, M.C. Stennett, C.L. Corkhill, P.G. Heath, R.J.Hand, M. James, A. Pearson, S. Morgan, J. Nucl. Mater., **444**, 186 (2014).
9. A.J. Connelly, N.C.Hyatt, K.P. Travis, R.J.Hand, M.C. Stennett, A.S. Gandy, A.P. Brown, D.C. Apperley, J. Non Cryst. Solids, **378**, 282 (2013).
10. M.C. Stennett, C.L. Freeman, A.S. Gandy, N.C. Hyatt, J. Solid State Chem., **192**, 172 (2012).
11. N.J. Cassingham, M.C. Stennett, P.A. Bingham, N.C. Hyatt, G. Aquilanti, Int. J. Appl. Glass Sci., **2**, 343 (2011).
12. P.A. Bingham, A.J.Connelly, N.J. Cassingham, N.C. Hyatt, J. Non Cryst. Solids, **357**, 2726 (2011).
13. A.J. Connelly, N.C. Hyatt, K.P. Travis, R.J. Hand, E.R. Maddrell, R.J. Short, J. Non Cryst. Solids, **357**, 1647 (2011).
14. D.P. Reid, M.C. Stennett, B. Ravel, J.C. Woicik, N. Peng, E.R. Maddrell, N.C. Hyatt, Nucl. Inst. Meth. Phys. Res. B, **268**, 1847 (2010).
15. R.J. Short, R.J. Hand, N.C. Hyatt, G, Mobus, J. Nucl. Mater., **340**, 179 (2005).
16. N.C. Hyatt, R.J. Short, R.J. Hand, W.E. Lee, F. Livens, J.M. Charnock, R.L. Bilsborrow, Ceramic Transactions, **168**, 179 (2005).
17. G.T. Seidler, D.R. Mortensen, A.J. Remesnik, J.I. Pacold, N.A. Ball, N. Barry, M. Styczinski, O.R. Hoidn, Rev. Sci. Instr., **85**, 113906 (2014).
18. D.R. Mortensen, G.T. Seidler, A.S. Ditter, P. Glatzel, J. Phys. Conf. Ser., **712**, 012036 (2016).
19. G.T. Seidler, A.S. Ditter, N.A. Ball, A.J. Remesnik, J. Phys. Conf. Ser., **712**, 012015 (2016).
20. E.P. Jahrman, W.M. Holden, A.S. Ditter, D.R. Mortensen, G.T. Seidler, T.T. Fister, S.A. Kozimor, L.F.J. Piper, J. Rana, N.C. Hyatt, M.C. Stennett, Rev. Sci. Instr., **90**, 024106 (2019).
21. A.P. Honkanen, S. Ollikkala, T. Ahopelto, A.J. Kallio, M. Blomberg, S. Huotari, Rev. Sci. Instr., 90, 033107 (2019).
22. C. Schlesiger, L. Anklamm, H. Stiel, W. Malzer, B. Kanngiesser, J. Anal. Atomic Spectr., **30**, 1080 (2015).
23. Z. Nemeth, J. Szlachetko, E.G. Bajnoczi, G. Vanko, Rev. Sci. Instr., **87**, 103105 (2016).
24. W. Malzer, G. Grotzsch, R. Gnewkow, C. Schlesiger, F. Kowalewski, B. Van Kuiken, S. DeBeer, B. Kanngiesser, Rev. Sci. Instr., **89**, 113111 (2018).
25. W. Blachucki, J. Czapla-Masztafiak, J. Sa, J. Szlachetko, J. Anal. Atomic Spectr., **34**, 1409 (2019).
26. F. Zeeshan, J. Hoszowska, L. Loperetti-Tornay, J.C. Dousse, Rev. Sci. Instr., **90**, 073105 (2019).
27. R.Bès, T.Ahopelto, A.-P.Honkanen, S.Huotari, G.Leinders, J.Pakarinen, K.Kvashnina, J. Nucl. Mater., 507, 50 (2018).
28. B. Ravel, M. Newville, J. Synch. Rad., **12**, 537 (2005).
29. J.A. Bearden, A.F. Burr, Rev. Mod. Phys., 39, 125 (1967).
30. M. C. Dixon Wilkins, M.C. Stennett, N.C. Hyatt, in review, MRS Advances (2019).
31. A. Bianconi, A. Marcelli, H. Dexpert, R. Karnatak, A. Kotani, T. Jo, J. Petiau, Phys. Rev. B, **35**, 806 (1987)
32. A. Soldatov, T. Ivanchenko, S. Dellalonga, A. Kotani, Y. Iwamoto, A. Bianconi, Phys. Rev. B, **50**,

5074 (1994).
33. D.P. Reid, M.C. Stennett, N.C. Hyatt, J. Solid State Chem., **191**, 2 (2012).
34. R.D. Shannon, Acta Cryst., **A32**, 751 (1976).
35. E. A. Stern and K. Kim, Phys. Rev. B, **23**, 3781 (1981).